JACS
JOURNAL OF THE AMERICAN CHEMICAL SOCIETY
Article
pubs.acs.org/JACS

Applying the Power of Reticular Chemistry to Finding the Missing alb-MOF Platform Based on the (6,12)-Coordinated Edge-Transitive Net

Zhijie Chen,[†] Łukasz J. Weseliński,[†] Karim Adil,[†] Youssef Belmabkhout,[†] Aleksander Shkurenko,[†] Hao Jiang,[†] Prashant M. Bhatt,[†] Vincent Guillerm,[†] Emilie Dauzon,[†] Dong-Xu Xue,[†] Michael O'Keeffe,[‡] and Mohamed Eddaoudi*,[†]

[†]Functional Materials Design, Discovery and Development Research Group (FMD^3), Advanced Membranes and Porous Materials Center (AMPMC), Division of Physical Sciences and Engineering (PSE), King Abdullah University of Science and Technology (KAUST), Thuwal 23955-6900, Kingdom of Saudi Arabia

[‡]School of Molecular Sciences, Arizona State University, Tempe, Arizona 85287, United States

Supporting Information

ABSTRACT: Highly connected and edge-transitive nets are of prime importance in crystal chemistry and are regarded as ideal blueprints for the rational design and construction of metal−organic frameworks (MOFs). We report the design and synthesis of highly connected MOFs based on reticulation of the sole two edge-transitive nets with a vertex figure as double six-membered-ring (d6R) building unit, namely the (4,12)-coordinated **shp** net (square and hexagonal-prism) and the (6,12)-coordinated **alb** net (aluminum diboride, hexagonal-prism and trigonal-prism). Decidedly, the combination of our recently isolated 12-connected (12-c) rare-earth (RE) nonanuclear $[RE_9(\mu_3\text{-}OH)_{12}(\mu_3\text{-}O)_2(O_2C-)_{12}]$ carboxylate-based cluster, points of extension matching the 12 vertices of hexagonal-prism d6R, with 4-connected (4-c) square porphyrinic tetracarboxylate ligand led to the formation of the targeted RE-**shp**-MOF. This is the first time that RE-MOFs based on 12-c molecular building blocks (MBBs), d6R building units, have been deliberately targeted and successfully isolated, paving the way for the long-awaited (6,12)-c MOF with **alb** topology. Indeed, combination of a custom-designed hexacarboxylate ligand with RE salts led to the formation of the first related **alb**-MOF, RE-**alb**-MOF. Intuitively, we successfully transplanted the **alb** topology to another chemical system and constructed the first indium-based **alb**-MOF, In-**alb**-MOF, by employing trinuclear $[In_3(\mu_3\text{-}O)(O_2C-)_6]$ as the requisite 6-connected trigonal-prism and purposely made a dodecacarboxylate ligand as a compatible 12-c MBB. Prominently, the dodecacarboxylate ligand was employed to transplant **shp** topology into copper-based MOFs by employing the copper paddlewheel $[Cu_2(O_2C-)_4]$ as the complementary square building unit, affording the first Cu-**shp**-MOF. We revealed that highly connected edge-transitive nets such **shp** and **alb** are ideal for topological transplantation and deliberate construction of related MOFs based on minimal edge-transitive nets.

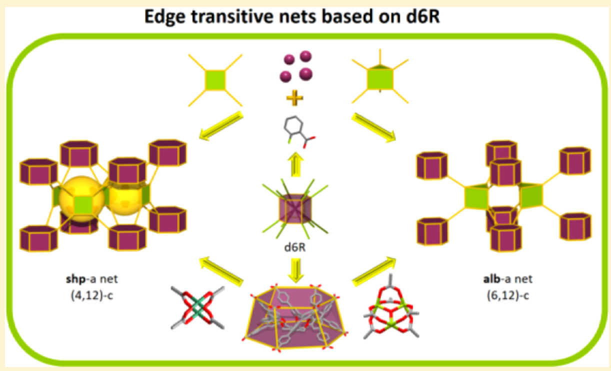

INTRODUCTION

Metal−organic frameworks (MOFs), hybrid materials encompassing metal-based nodes (metal ions or metal clusters) linked by polytopic organic ligands (linkers), are acknowledged as an important class of functional solid-state materials with unrivaled scientific interest in academia and industry alike.[1] Their modular nature (e.g., structural and compositional diversity, tunable functionality, high surface area, adjustable pore system, etc.) renders MOFs as prospective materials to address various persistent challenges pertaining to gas storage/separation,[2] catalysis,[3] drug delivery,[4] and smart sensing.[5] Markedly, the development of new MOF platforms necessitates (i) the isolation of reaction conditions that permit the in situ formation of the requisite inorganic molecular building block (MBB), and (ii) its subsequent reticulation into a MOF with the targeted net topology by the judicious selection of a suitable polytopic organic ligand with the appropriate shape, geometry, and connectivity.[6]

The MBB approach has already been successfully demonstrated for the design, directed-assembly, and development of solid-state porous materials.[6a,b] The MBB approach has emerged as a prominent avenue toward the design and construction of novel functional materials—that is, desired functionality and properties can be introduced in preselected MBBs at the design stage, prior to the assembly process. Evidently, the potential for design is directly correlated to the ability to envision the resultant

Received: January 7, 2017
Published: February 5, 2017

DOI: 10.1021/jacs.7b00219
J. Am. Chem. Soc. 2017, 139, 3265−3274

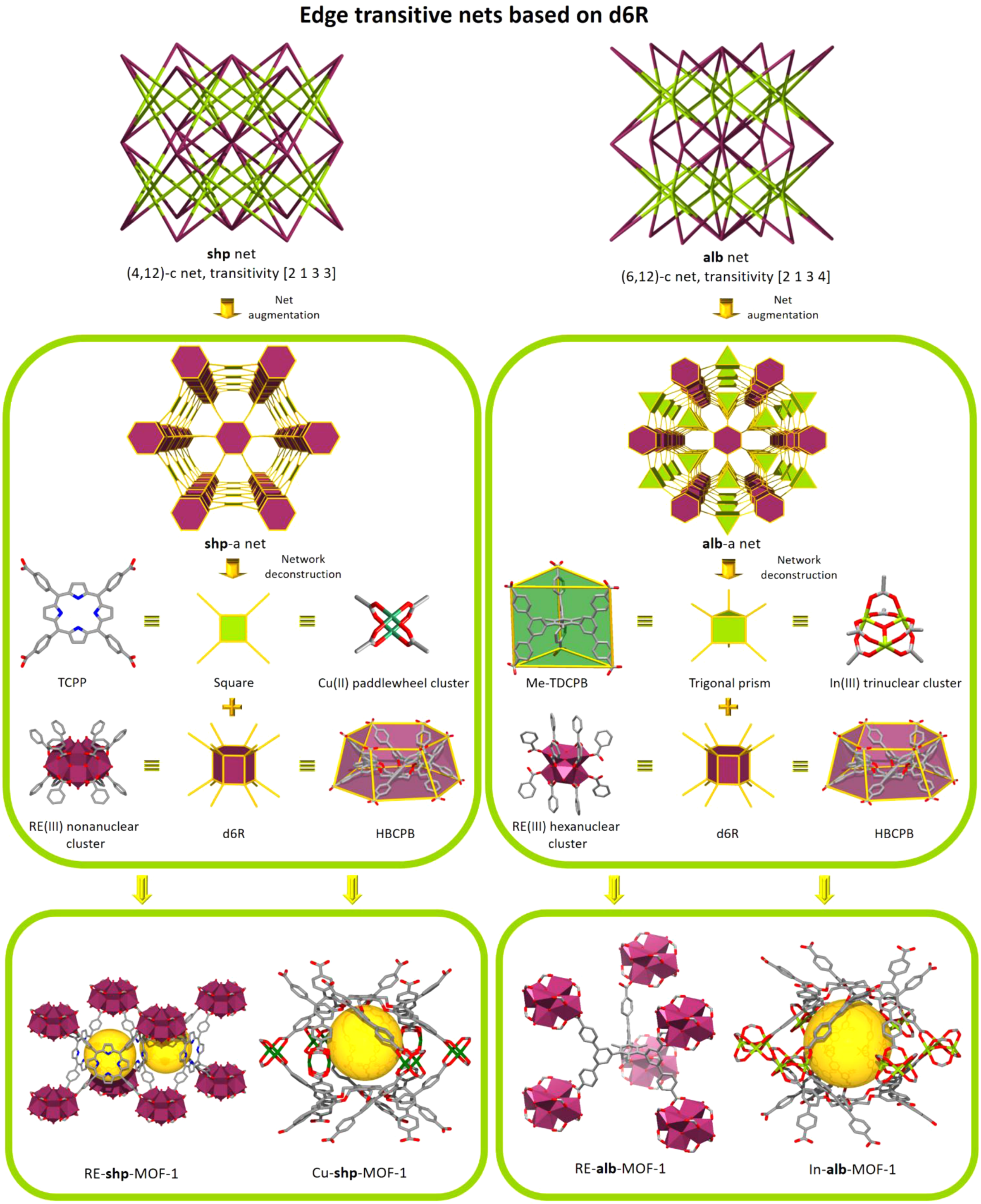

Figure 1. Road map for the top-down design and bottom-up assembly of highly connected MOFs with the sole two edge-transitive nets based on d6R, square hexagonal-prism (**shp**) and aluminum diboride (**alb**). RE, Cu, In, C, O, and N are represented by purple, green, lime, gray, red, and blue, respectively, and H atoms and solvent molecules are omitted for clarity. RE atoms are represented as polyhedra.

structure topology on the basis of the available information pertinent to the geometry and connectivity of the preselected/targeted building blocks. Plausibly, incorporation of the desired directional and structural information into the employed building blocks offers the potential to readily access the net-coded building units (**net**-cBUs), where precise embedded geometrical information uniquely codes a selected net.[6d]

DOI: 10.1021/jacs.7b00219
J. Am. Chem. Soc. 2017, 139, 3265−3274

Credibly, edge-transitive nets (all edges are equivalent by symmetry) are regarded as suitable targets in crystal chemistry.[7] In particular, highly connected nets with at least one *n*-connected node, where $n \geq 12$, emerge as ideal blueprints to pursue and deploy in MOF crystal chemistry, as the assembly of highly connected building blocks offers great prospects to limit/reduce the number of reasonable outcome nets.[6c,8] Nevertheless, highly connected MBBs (*n*-connected, where $n \geq 12$) are scarce, mainly due to the fact that MBBs with corresponding high connectivity are too intricate to realize/apprehend as polynuclear clusters or polycarboxylate ligands. Propitiously, our ongoing efforts toward the discovery of highly coordinated MBBs, and their reticulation into novel MOF platforms, had permitted the introduction of highly connected rare-earth (RE) polynuclear clusters, assembled *in situ* in the presence of fluorinated ligands and/or modulators such as 2-fluorobenzoic acid (2-FBA), for the design and construction of highly connected RE-MOFs.[6c,8a,9]

Isolation of the 12-connected (12-c) rare-earth (RE) nonanuclear $[RE_9(\mu_3\text{-}OH)_{12}(\mu_3\text{-}O)_2(O_2C-)_{12}]$ carboxylate-based cluster, points of extension matching the 12 vertices of the hexagonal-prism (double six-membered ring, d6R), paves the way toward the design and discovery of new RE-MOF platforms based on the logical reticulation of d6R building blocks.[9b] Appreciably, the Reticular Chemistry Structural Resource (RCSR) database contains only two binodal edge-transitive nets with a vertex figure as a double six-membered-ring (d6R) building unit, namely the (4,12)-coordinated **shp** net (square and hexagonal-prism) and the (6,12)-coordinated **alb** net (aluminum diboride, hexagonal-prism and trigonal-prism) (Figure 1).[10] Rationally, the ability of RE polynuclear clusters to form d6R inspired us to target the construction of RE-MOF platforms based on the reticulation of the sole binodal edge-transitive nets based on d6R building units. It should be mentioned that these d6R MBBs have not yet been used to construct highly connected binodal nets (n_1,n_2-connected, where $n_1 \geq 6$, $n_2 \geq 12$), i.e., the edge-transitive (6,12)-c **alb**-net, which is the only possible net constructed from trigonal-prism and d6R hexagonal-prism building units.[10b] To the best of our knowledge, no carboxylate-based **alb**-MOFs have been reported so far in the open literature, plausibly due to the difficulty to generate and concomitantly combine the 6-c and 12-c MBBs.[11]

To tackle the prospective design and rational construction of the missing **alb**-MOF platform based on the (6,12)-coordinated edge-transitive net, we delineated several key prerequisites: (i) 6-connected (6-c) trigonal-prismatic MBBs, which can be inorganic trinuclear clusters[12] or dendritic polycarboxylate ligands;[13] (ii) 12-c hexagonal-prismatic (d6R) MBBs, which can be our recently discovered polynuclear clusters or novel polycarboxylate ligands matching the vertex figure of the d6R building unit; and (iii) reaction conditions that permit the attainment of single-crystalline materials for the combination of highly connected inorganic and organic MBBs, conferring the definitive structural analysis.

In this contribution, we describe the design and construction of a series of highly stable RE porphyrinic **shp**-MOFs based on the assembly of 12-c nonanuclear carboxylate-based MBBs, displaying rare d6R building units, and 4-connected (4-c) tetratopic ligands. Notably, we also report the rational design and deliberate assembly of the long-awaited (6,12)-c **alb**-MOFs (i.e., RE-**alb**-MOF-1 and In-**alb**-MOF-1). The predesigned hexacarboxylate ligand, resembling the requisite trigonal-prism, 2,4,6-trimethyl-1,3,5-tri(3,5-di(4-carboxyphenyl-1-yl)phenyl-1-yl)-benzene (H_6Me-TDCPB), guided the formation of the RE hexanuclear carboxylate-based cluster $[RE_6(\mu_3\text{-}OH)_8(2\text{-}FBzoate)_2(H_2O)_2(O_2C-)_{12}]$ (RE = Y, Tb) as a 12-c d6R MBB and the formation of the first 3-periodic RE-**alb**-MOF-1 (2-fluorobenzoate (2-FBzoate) = $C_7H_4FO_2$). Intuitively, we successfully transplanted the **alb** topology to another chemical system and constructed the first indium-based **alb**-MOF, In-**alb**-MOF-1, by employing the trinuclear $[In_3(\mu_3\text{-}O)(O_2C-)_6]$ carboxylate-based cluster as the requisite 6-c trigonal-prism building unit and a purposely made dodecacarboxylate ligand as a compatible 12-c MBB, 1,2,3,4,5,6-hexakis[3,5-bis(4-carboxylphenyl)phenoxymethyl]benzene (H_{12}HBCPB), plausibly affording the positioning of the carbon centers of the 12 carboxylate groups on the vertices of the desired hexagonal-prism building unit.

It is worth mentioning that In-**alb**-MOF-1 represents the first example of **alb**-MOFs based on the assembly of a metal trinuclear cluster and a dodecacarboxylate ligand. The successful construction of this first In-**alb**-MOF is the immediate result of the rational practice of reticular chemistry in combination with the understanding and deployment of net-coded building units (**net**-cBUs). Precisely, two MOFs related to the same parent **alb** topology, based on the combination of trigonal-prism and hexagonal-prism **net**-cBUs, were constructed by carrying out a topological transplantation, where building blocks in one **alb**-MOF (RE-**alb**-MOF-1, the 6-c hexacarboxylate organic ligands and the 12-c inorganic RE polynuclear clusters) were replaced by chemically different but topologically related building blocks to construct a second **alb**-MOF (In-**alb**-MOF-1, from the 6-c inorganic indium trinuclear clusters and 12-c dodecacarboxylate organic ligands). This deliberate and effective topological transplantation illustrates (i) the prospective employment of branched ligands as a credible pathway to access the requisite and intricate highly coordinated **net**-cBUs; (ii) the benefits of considering **net**-cBUs as a rational and a viable pathway for the design and construction of 3-periodic MOFs; and (iii) the prominence of highly connected edge-transitive nets such **shp** and **alb** nets as ideal blueprints for the topological transplantation and the design and deliberate construction of related MOFs based on minimal edge-transitive nets. The ability of the newly synthesized dodecacarboxylate ligand to mimic the d6R, by peripherally exposing the 12 carboxylates to resemble the requisite hexagonal-prism building unit, was employed to transplant the **shp** topology into a copper-based MOF by employing the copper paddlewheel $[Cu_2(O_2C-)_4]$ cluster as the complementary square building unit, thus accomplishing the construction of the first Cu-**shp**-MOF.

Interestingly, the RE-**alb**-MOF-1 structure displays a flexible behavior upon exposure to various gases, depending on the nature of the adsorbed gas and associated pressure. Accordingly, the RE-**alb**-MOF platform can be regarded as a highly connected third generation of flexible MOFs.

■ RESULTS AND DISCUSSION

RE-shp-MOF-1 Platform. At the outset of this study, the recently isolated 12-c rare-earth nonanuclear $[RE_9(\mu_3\text{-}OH)_{12}(\mu_3\text{-}O)_2(O_2C-)_{12}]$ carboxylate-based cluster, points of extension matching the 12 vertices of the hexagonal-prism (d6R),[9b] was employed in combination with the 4-c square porphyrinic tetracarboxylate ligand in order to direct the formation of the (4,12)-c MOF with the targeted **shp** underlying topology.

Indeed, reactions between $Y(NO_3)_3 \cdot 6H_2O$ and 5,10,15,20-tetrakis(4-carboxyphenyl)porphyrin (H_4TCPP) in the presence of 2-FBA in an *N*,*N*′-dimethylformamide (DMF)/water solution yielded dark red rod-shaped crystals, formulated by single-crystal X-ray diffraction study (SCXRD) as $|(DMA)_5|[Y_9(\mu_3\text{-}O)_2(\mu_3\text{-}OH)_{12}(OH)_4(H_2O)_5(TCPP)_3]\cdot(solv)_x$ (**1**) (DMA = dimethylammonium cation and solv = solvent) (Table S1). Compound **1** crystallizes in the hexagonal space group *P6*/*mmm*. The anticipated nonanuclear cluster is observed in **1** and is disordered over two positions (Figure 1 and Figure S2). Three of the yttrium ions are each coordinated to four μ_3-OH and four oxygens from carboxylates, leaving the ninth coordination site occupied by a water molecule, while each of the other six yttrium ions is surrounded by one μ_3-O, four μ_3-OH, two oxygens from carboxylates, and one water or OH molecule. The overall cluster is anionic, $[Y_9(\mu_3\text{-}O)_2(\mu_3\text{-}OH)_{12}(OH)_4(H_2O)_5(O_2C-)_{12}]^{5-}$, and the resultant framework's overall charge is balanced by five DMA cations generated *in situ* from the decomposition of DMF solvent molecules.

Structural and topological analysis of the resulting crystal structure revealed the formation of the anticipated (4,12)-c MOF based on a polynuclear RE cluster, $[Y_9(\mu_3\text{-}O)_2(\mu_3\text{-}OH)_{12}(OH)_4(H_2O)_5(O_2C-)_{12}]$, a distinctive 12-c MBB, linked to the square TCPP to form a 3-periodic MOF with the underlying **shp** topology, Y-**shp**-MOF-1 (Figure S3). The carbon atoms of the coordinated carboxylate moieties and the *meso*-positions of porphyrin rings, acting as points of extension, coincide with the respective d6R and square vertex figures of the **shp** net, the sole binodal edge-transitive net for the assembly of square and hexagonal-prism building units.

As anticipated, substitution of the yttrium metal salt with $Tb(NO_3)_3\cdot 5H_2O$ under similar reaction conditions resulted in the analogous Tb-**shp**-MOF-1, $|(DMA)_5|[Tb_9(\mu_3\text{-}O)_2(\mu_3\text{-}OH)_{12}(OH)_4(H_2O)_5(TCPP)_3]\cdot(solv)_x$ (**2**), confirmed by SCXRD and powder X-ray diffraction (PXRD) data (Table S4 and Figure S20).

Compound **1** contains triangular one-dimensional channels with a diameter of ca. 11 Å (considering van der Waals (vdW) radii) along the *c*-axis. The framework of **1** encloses one kind of hexagonal-prismatic cage having diameters of ca. 10.4 Å (height) and ca. 9.9 Å (width) and can accommodate an estimated 9.9 Å sphere including vdW radii. The hexagonal-prismatic cage is generated by six different TCPP ligands and two nonanuclear RE clusters (Figure S2). The corresponding solvent-accessible free volume for **1** was estimated to be 58.5% by summing voxels more than 1.2 Å away from the framework using PLATON software.[14]

The phase purity of the bulk crystalline materials for **1** was confirmed on the basis of similarities between the calculated and as-synthesized PXRD patterns (Figure S19). Moreover, variable-temperature powder X-ray diffraction (VT-PXRD, Figure S26) and thermogravimetric analysis (TGA, Figure S20) show that **1** has remarkable thermal stability. Solid-state ultraviolet−visible (UV−vis) and Fourier transform infrared (IR) measurements revealed that the TCPP linker was not metalated after synthesis (Figure S32).

The permanent porosity of **1** has been confirmed by an argon adsorption isotherm at 87 K (Figures S35 and S36), showing a fully reversible type-I isotherm characteristic of a microporous material with permanent porosity. The apparent Brunauer−Emmett−Teller (BET) and Langmuir surface area of **1** were estimated to be 2200 and 2360 $m^2\cdot g^{-1}$, respectively. The experimental total pore volume obtained from the Ar adsorption isotherm was estimated to be 0.79 $cm^3\cdot g^{-1}$, which is in good agreement with the theoretical pore volume of 0.90 $cm^3\cdot g^{-1}$, based on the associated crystal structure.

Since Y^{3+} failed to metalate the porphyrin during the synthesis of compound **1**, the porphyrin remained as a free base, available for presynthetic, *in situ*, and postsynthetic metalation procedures. Plausibly, the exposed periodic array of the porphyrin centers along the 1D channels in **1** can potentially be functionalized via metalation using various metal cations. As a matter of fact, metalation of **1** using Fe^{3+}, Zn^{2+} was successful, as confirmed by SCXRD (Tables S2 and S3), atomic analysis from inductively coupled plasma optical emission spectrometry (ICP-OES) (Table S9), and solid-state UV−vis as well as IR spectroscopies (Figures S33 and S34). As expected, crystal structures of the metalated analogues crystallize in the hexagonal space group *P6*/*mmm*, maintaining the same structure as the **shp** topology. Phase purity of bulk materials was further confirmed on the basis of similarities between the calculated and as-synthesized PXRD patterns, while thermal stabilities were also examined using TGA and VT-PXRD techniques (Figures S21, S22, S27, and S28), showing high thermal stability similar to that of the parent material **1**.

Accordingly, the porosity of **1-M** (M = Fe, Zn) has been confirmed by Ar adsorption (Tables S10 and S11, Figures S38 and S41). The apparent BET surface areas of **1-Fe** and **1-Zn** were estimated to be 2030 and 2360 $m^2\cdot g^{-1}$, respectively. The experimental total pore volumes of **1-Fe** and **1-Zn** obtained from Ar adsorption isotherms were estimated to be 0.75 and 0.85 $cm^3\cdot g^{-1}$, respectively. Interestingly, the isosteric heat of adsorption (Q_{st}) of CO_2, estimated by applying the Clausius−Clapeyron equation using the CO_2 isotherms measured at 253, 273, 288, and 298 K, was enhanced from 25.2 to 31.8 and 34.6 $kJ\cdot mol^{-1}$ at low loading for **1**, **1-Fe**, and **1-Zn**, respectively (Figures S37, S40, and S43). This noticeable enhancement can be attributed to the presence of favorable adsorption metal sites within the metalloporphyrin-based **shp**-MOFs. In light of the high porosity of **shp**-MOFs, high-pressure CH_4 and CO_2 adsorption studies were conducted on the **1** and **1-Zn**. Examination of excess and absolute CH_4 gravimetric ($cm^3(STP)\cdot g^{-1}$) (Figure S48) and volumetric ($cm^3(STP)\cdot cm^{-3}$) (Figure S49) uptakes at intermediate and high pressures showed that **1-Zn** exhibits much higher CH_4 adsorption capacity than the parent nonmetalated analogue **1** over the entire evaluated pressure range at room temperature. **1-Zn** adsorbs 179, 232, and 249 $cm^3(STP)\cdot cm^{-3}$ of CH_4 at 35, 65, and 80 bar, respectively. Consequently, the resulting CH_4 working storage capacities, assuming 35, 65, and 80 bar as the highest adsorption pressure and 5 bar as the lowest desorption pressure, are ca. 129, 182, and 199 $cm^3(STP)\cdot cm^{-3}$, respectively. The recorded value for the 5−80 bar range is among the highest methane storage working capacities, slightly below the corresponding values for MOF-519,[15] UTSA-76a,[16] Al-**soc**-MOF-1,[6b] and HKUST-1[17] (Table S12). Interestingly, the Q_{st} of CH_4 adsorption for **1-Zn**, determined from variable low-pressure data (Figure S44), was estimated to be ca. 14 $kJ\cdot mol^{-1}$ at low CH_4 loading, and it remained remarkably steady even at higher CH_4 loading. In fact, this shows that the CH_4 interaction with the framework of **1-Zn** is very mild and uniform in comparison to other CH_4 storage media[18] and mostly governed by the pore filling and the CH_4−CH_4 interactions at high relative pressures.

Analysis of CO_2 adsorption for these compounds at high pressure (Figure S50) shows that **1-Zn** exhibits a very high CO_2 volumetric uptake at 25 bar (307 $cm^3(STP)\cdot cm^{-3}$). The CO_2 volumetric uptake represents one of the highest volumetric CO_2 adsorption uptake values reported in the literature (Table S13).

RE-alb-MOF-1 Platform. This is the first time that RE-MOFs, namely RE-**shp**-MOFs, based on 12-c MBBs, as d6R

DOI: 10.1021/jacs.7b00219
J. Am. Chem. Soc. 2017, 139, 3265−3274

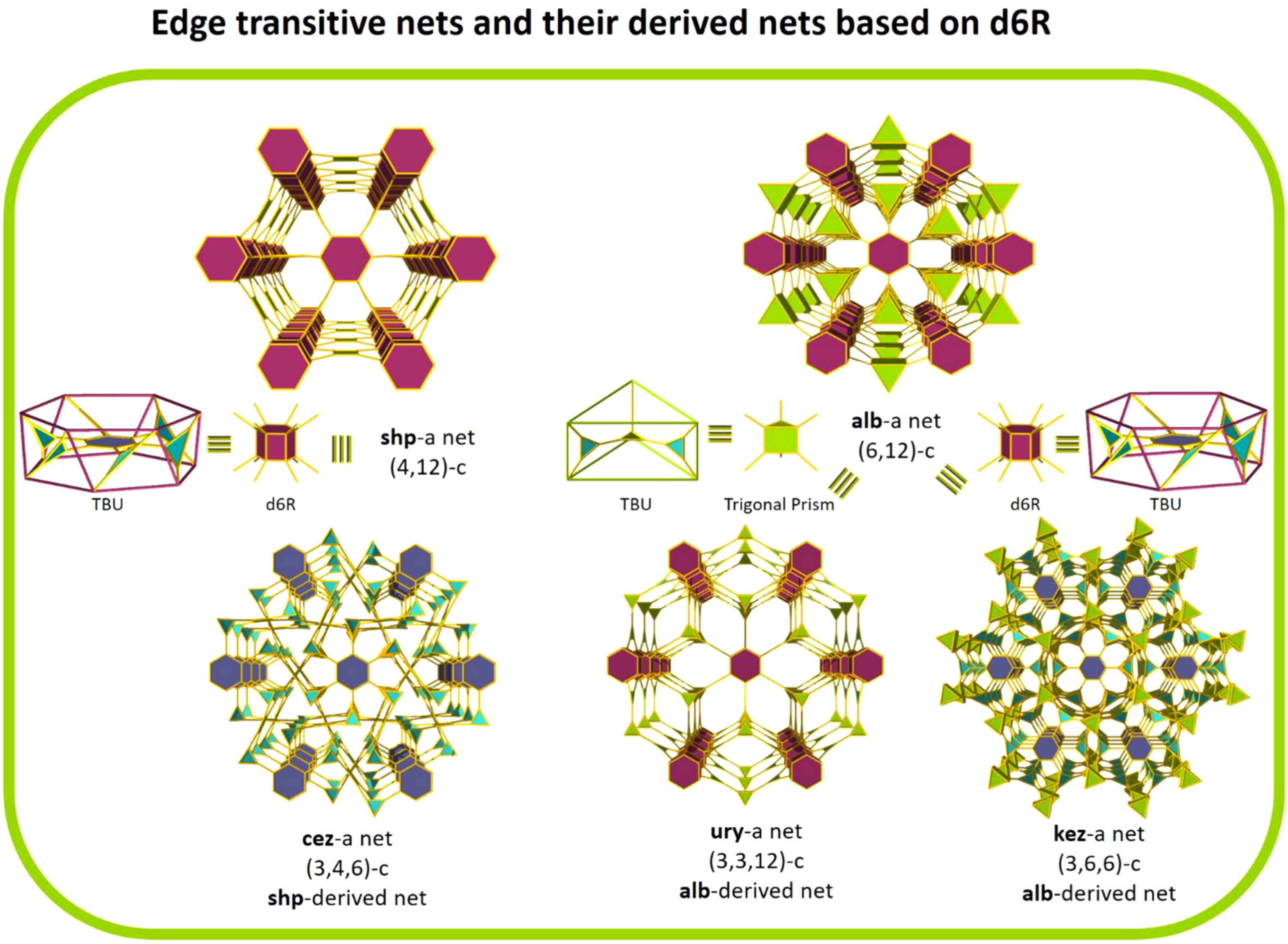

Figure 2. Two edge-transitive nets based on d6R (square hexagonal-prism (**shp**) and aluminum diboride (**alb**) net) and their derived minimal edge-transitive nets. For clarity, **shp**, **alb**, **cez**, **ury**, and **kez** topologies are represented as augmented nets.

building units, have been deliberately targeted and successfully isolated, paving the way for the isolation of the other long-awaited (6,12)-c MOFs with the underlying **alb** topology. Importantly, **alb** is the only binodal edge-transitive net, with its two distinct vertex figures matching the trigonal-prism and the hexagonal-prism. A custom-designed hexacarboxylate ligand, where the carbon centers of the six carboxylate groups coincide with the vertices of the trigonal-prism, was synthesized, and its combination with RE metal salts in the presence of 2-FBA is anticipated to lead to the formation of the first related **alb**-MOF based on 12-c hexanuclear RE clusters with the desired (6,12)-c **alb** topology, RE-**alb**-MOF.

Indeed, reactions between $Y(NO_3)_3 \cdot 6H_2O$ and 2,4,6-trimethyl-1,3,5-tri(3,5-di(4-carboxyphenyl-1-yl)phenyl-1-yl)-benzene (H_6Me-TDCPB),[13b] in the presence of 2-FBA in a DMF/chlorobenzene/water solution, yielded colorless block-shaped crystals, formulated by SCXRD study as $|(DMA)_4|[Y_6(\mu_3\text{-}OH)_8(2\text{-FBzoate})_2(H_2O)_2(\text{Me-TDCPB})_2]\cdot(\text{solv})_x$ (Y-**alb**-MOF-1) (Table S5 and Figure S4). The SCXRD structure indicated that compound **3** crystallizes in the monoclinic space group $P2/m$. Analysis of the resultant crystal structure of **3** revealed the *in situ* formation of highly connected yttrium polynuclear carboxylate-based hexanuclear clusters and their subsequent assemblage by the fully deprotonated hexa-carboxylate ligands (referred to as Me-TDCPB) to yield a novel 3-periodic highly connected MOF. The central phenyl ring of the ligand Me-TDCPB is orthogonal/vertical to the other three adjacent ones, due to the steric hindrance enforced by the methyl groups.

Analysis of the Y hexanuclear cluster reveals that two Y^{3+} cations are each coordinated to nine oxygen atoms: that is, four carboxylates from four separate Me-TDCPB ligands, four μ_3-OH, and one terminal water molecule. The remaining four Y^{3+} cations are each coordinated to eight oxygen atoms: namely, four from the carboxylates of the three independent Me-TDCPB ligands, and the remaining four from bridging μ_3-OH and disordered terminal ligands (2-FBzoate). Concisely, the resultant hexanuclear cluster, $[Y_6(\mu_3\text{-}OH)_8(2\text{-FBzoate})_2(H_2O)_2(O_2C-)_{12}]$, is capped by 12 carboxylates from 12 different Me-TDCPB ligands (Figure 1) and 2 carboxylates from 2 terminal 2-FBzoate ligands to give a 12-c MBB, $[Y_6(\mu_3\text{-}OH)_8(O_2C-)_{12}]$, with points of extension corresponding to the carbons of the carboxylate moieties from 12 distinct hexacarboxylate ligands and matching the d6R vertex figure of a fully symmetrical 12-c node.

Topological analysis of the resulting crystal structure reveals that the combination of the aforementioned 12-c MBB, $[Y_6(\mu_3\text{-}OH)_8(O_2C-)_{12}]$, and the 6-c organic MBB, Me-TDCPB ligand, resulted in the formation of a highly connected MOF, reticulating the (6,12)-c net with the **alb** underlying topology, Y-**alb**-MOF-1 (**3**) (Figure 1 and Figures S10 and S11). Interestingly, the constrained geometry of the ligand Me-TDCPB did not promote the construction of the **alb**-MOF based on the targeted Y nonanuclear cluster but prompted the

DOI: 10.1021/jacs.7b00219
J. Am. Chem. Soc. 2017, 139, 3265−3274

formation of a new Y hexanuclear carboxylate-based cluster with 12 connecting carboxylates as points of extension and enabling the formation of the RE-**alb**-MOF. It is worth noting that this is the first example of a RE hexanuclear carboxylate-based cluster acting as a d6R MBB, manifested in a given MOF and that can be further employed/targeted for the prospective construction of other highly connected MOFs.

From a purely topological point of view, the binodal **alb** edge-transitive net, with only one kind of edge, has the transitivity [2134]. Alternatively, the Y-**alb**-MOF-1 structure can be described as the **ury** topology: (3,3,12)-c trinodal net with minimal transitivity [3234] (Figures S12, S13, and S17), where the ligand can be further deconstructed into two distinct 3-c nodes (Figure 2). It is to be noted that the **ury** net is an **alb**-derived net; that is, **alb** net is the parent net, and the **ury** net is derived from the **alb** net by replacing the 6-c nodes by two kinds of 3-c nodes.

As anticipated, replacement of the yttrium metal salt with $Tb(NO_3)_3 \cdot 5H_2O$ under similar reaction conditions resulted in the analogous Tb-**alb**-MOF-1, $|(DMA)_4|[Tb_6(\mu_3\text{-}OH)_8(2\text{-}FBzoate)_2(H_2O)_2(Me\text{-}TDCPB)_2]\cdot(solv)_x$ (**4**) (Table S6 and Figure S24).

Interestingly, close examination of the RE-**alb**-MOF-1 structure revealed that it is built from pillared hexagonal lattice (**hxl**) layers (Figure 3). Explicitly, the hexanuclear cluster MBBs

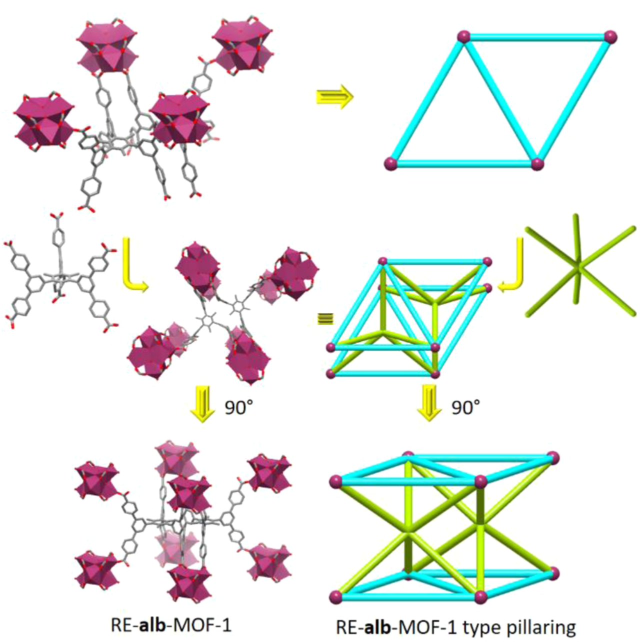

Figure 3. Schematic showing the RE-**alb**-MOF-1 pillaring type observed in RE-**alb**-MOF-1. RE, C, and O are represented by purple, gray, and red, respectively, and H atoms and solvent molecules are omitted for clarity.

arrange to form 2-periodic **hxl** layers in the *ab* plane, pillared by Me-TDCPB ligands, thus resulting in a 3-periodic MOF. Compound **3** contains one kind of zigzag-shaped one-dimensional channels perpendicular to the *c*-axis. These zigzag channels were cross-linked to form the honeycomb (**hcb**)-shaped channels in the *ab*-plane with diameters of ca. 14.1 Å (height) and ca. 11.7 Å (width) and a quadrangular window (ca. 12.7 × 3.8 $Å^2$) including vdW radii (Figure S6). Additionally, compound **3** also comprises quadrangular narrow channels (ca. 6.4 × 3.4 $Å^2$ considering vdW radii) along the *c*-axis. Compound **3** encompasses one kind of hexagonal-prismatic cages enclosed by six different Me-TDCPB ligands and two hexanuclear RE clusters (Figure S7). The corresponding solvent-accessible free volume for **3** was estimated to be 3094.6 $Å^3$ (52.5% of the unit cell volume of 5893.7 $Å^3$) by summing voxels more than 1.2 Å away from the framework using PLATON software.[14]

The phase purity of the bulk crystalline material for **3** was confirmed on the basis of similarities between the calculated and as-synthesized PXRD patterns (Figure S23). TGA (Figure S23) was carried out under N_2 atmosphere and revealed that the framework of compound **3** is stable up to at least 250 °C. VT-PXRD studies under vacuum or in the open atmosphere suggested the Y-**alb**-MOF-1 (**3**) maintains its crystallinity after solvent removal (Figure S29). Close examination of the VT-PXRD patterns revealed a slight shift in the peak positions at lower angles, suggesting the framework contracts upon solvent removal under heat. The original PXRD patterns of the as-synthesized material can be regenerated/recovered by immersing the desolvated form of **3** in DMF (Figure S30). These results corroborate that the contraction−swelling of the Y-**alb**-MOF-1 is reversible and directly controlled by removal and reintroduction of guest molecules. It is to be noted that the same behavior was observed for Tb-**alb**-MOF-1 (**4**) (Figure S31).

In-alb-MOF-1 Platform. Intuitively, the (6,12)-c **alb** net is an ideal blueprint for the design of MOFs, since the **alb** net is the sole edge-transitive net based on the trigonal-prism and the hexagonal-prism building units. That is to say, that net-coded building units (**net**-cBUs) for the **alb** net are the trigonal-prism (**alb**-cBU-1) and the hexagonal-prism (**alb**-cBU-2). In principle, the predisposition of a 6-c MBB with a trigonal-prism geometry and a 12-c MBB with the hexagonal-prism geometry will permit their prospective assembly into the **alb** net. Accordingly, we aimed to put this approach into practice and thus aspired to transplant the **alb** topology to another chemical system. RE-**alb**-MOF-1 was successfully constructed by combining the 6-c hexacarboxylate organic ligand as the requisite trigonal-prism (**alb**-cBU-1) and the 12-c inorganic RE polynuclear cluster as the complementary hexagonal-prism (**alb**-cBU-2). Our proposed approach is to alter the nature and composition of the **alb**-cBUs and employ a 6-c inorganic cluster as the **alb**-cBU-1 and a 12-c dodecacarboxylate organic ligand as the **alb**-cBU-2 (Figure 1).

Implementation of this approach requires the design of a new organic ligand (in this case, to replace the 12-c RE cluster) to act as a 12-c building block and the employment of the trinuclear $[In_3(\mu_3\text{-}O)(O_2C-)_6]$ carboxylate-based cluster as the requisite 6-c trigonal-prism building unit (replacing the 6-c ligand in the RE-**alb**-MOF-1). Virtually, the 12-c dense d6R-shaped RE cluster in the RE-**alb**-MOF-1 can be substituted elegantly with a relatively open organic MBB, while the custom-designed organic trigonal-prism-like ligand can be replaced by a comparatively smaller inorganic trimer building block. The key requirement to translate the augmented **alb** (**alb**-a) net into practice for MOF chemistry is to purposely make a dodeca-carboxylate ligand that can act as a compatible 12-c MBB and plausibly afford the positioning of the carbon centers of the 12 carboxylate groups on the vertices of the desired hexagonal-prism building unit (Figure 1).

Indeed, reactions between $In(NO_3)_3 \cdot 2H_2O$ and 1,2,3,4,5,6-hexakis[3,5-bis(4-carboxylphenyl)phenoxymethyl]benzene ($H_{12}HBCPB$) in DMF/acetonitrile solution yielded colorless rod-shaped crystals, formulated by SCXRD study as $[(In_3O)_2(C_{132}O_{30}H_{78})(O_2CH)_2(H_2O)_4]\cdot(solv)_x$ (In-**alb**-MOF-1) (**5**) (Table S7 and Figure S5). SCXRD study discloses that

DOI: 10.1021/jacs.7b00219
J. Am. Chem. Soc. 2017, 139, 3265−3274

compound **5** crystallizes in the hexagonal space group *P*6/*m*. Analysis of the resultant crystal structure of **5** revealed the *in situ* formation of the 6-c indium trinuclear cluster building block, $[In_3(\mu_3\text{-}O)(O_2C-)_6]$, linked by six separate fully deprotonated dodecacarboxylate ligands (HBCPB) to yield a novel 3-periodic highly connected In-based MOF (In-**alb**-MOF-1) (Figure 1). The trinuclear clusters contain three $[InO_6]$ octahedra sharing one central μ_3-oxo anion. In each $[InO_6]$ octahedron, the apical position is occupied by a terminal water molecule or a formate anion, generated *in situ* from the decomposition of DMF solvent molecules. In the crystal structure of **5**, each indium is trivalent, yielding an overall neutral framework.

Topological analysis of the resulting crystal structure revealed that the deliberate combination of the aforementioned 6-c MBB, $[In_3(\mu_3\text{-}O)(O_2C-)_6]$, and the 12-c organic MBB, HBCPB ligand, resulted as planned/expected in the formation of a highly connected MOF, In-**alb**-MOF-1, based on the reticulation of the (6,12)-c net with **alb** underlying topology (Figure 1 and Figure S14). Noticeably, the arms of the 12-c organic ligand are not perpendicular to the central benzene core, and the dihedral angle between the benzene core and plane of the ligand arms is around 45°, eventually resulting in points of extension of the 12-c MBB to coincide with the vertices of the hexagonal-prism, the 12-c vertex figure of the **alb** net. From a purely topological point of view, this structure can alternatively be termed as the newly discovered **kez** topology: a (3,6,6)-c trinodal net with minimal transitivity [32] (Figures S15, S16, and S18), where the ligand can be further deconstructed into one kind of 3-c node and one 6-c node. This novel **kez** topology represents a new type of **alb**-derived nets.

To the best of our knowledge, this represents the first example of MBB transposition in highly *n*-connected MOFs with at least one node higher than 8-connected; namely, highly connected MBBs in RE-**alb**-MOF-1 (the 6-c hexacarboxylate organic ligands and the 12-c inorganic RE polynuclear clusters) are replaced by chemically different but topologically related MBBs to In-**alb**-MOF-1 (the 6-c inorganic indium trinuclear clusters and 12-c dodecacarboxylate organic ligands).

Interestingly, close inspection of the In-**alb**-MOF-1 structure revealed that it is built from pillared **hcb** layers (Figure 4). The indium trimer MBBs assemble to generate a 2-periodic **hcb** layer in the *ab* plane, pillared by 12-c HBCPB ligands, thus resulting in a 3-periodic framework. Compound **5** contains one kind of zigzag-shaped one-dimensional channels. The framework of **5** encompasses one kind of hexagonal-prismatic cage enclosed by two different HBCPB ligands and six In trimers (Figure S8). The hexagonal-prismatic cage displays two types of conformations due to the flexibility of the central benzene core of the ligand, having diameters of ca. 20.5 Å (width) and ca. 5.2 or 12.9 Å (length) considering vdW radii. Remarkably, these cages were cross-linked through quadrangular windows to generate the **hxl** channels in the *ab*-plane of the crystal structure, reminiscent of the observed **hxl** cluster-based layers in the RE-**alb**-MOF-1 (Figure S9). It can be appreciated that the **hcb** trimer-based layers observed in the In-**alb**-MOF-1 are related to the **hcb** channels occurring in the RE-**alb**-MOF-1, corroborating the relation between the two **alb**-MOFs based on different **alb**-derived nets; that is, the **ury** net and **kez** net are directly related and are both derived from the same parent **alb** net.

The corresponding solvent-accessible free volume for **5** was estimated to be 19 927.8 Å^3 (60.6% of the unit cell volume of 32 866.6 Å^3) by summing voxels more than 1.2 Å away from the framework using PLATON software.[14]

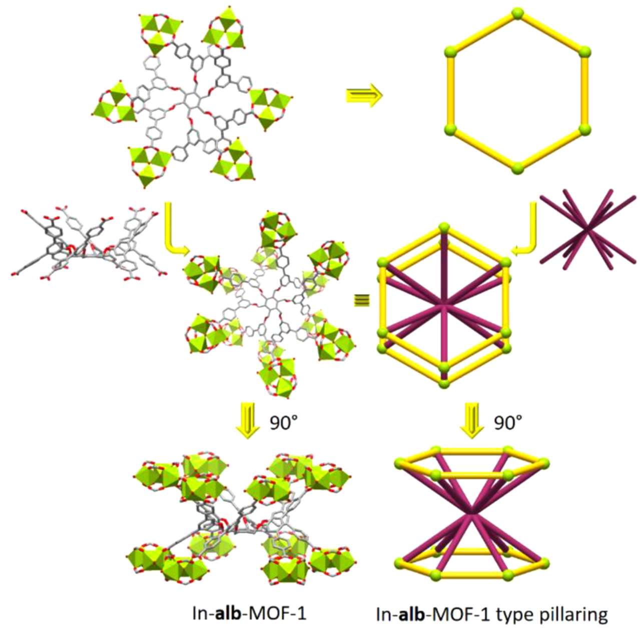

Figure 4. Schematic showing the In-**alb**-MOF-1 pillaring type observed in In-**alb**-MOF-1. In, C, and O are represented by lime, gray, and red, respectively, and H atoms and solvent molecules are omitted for clarity.

The phase purity of the bulk crystalline material for **5** was confirmed on the basis of similarities between the calculated and as-synthesized PXRD patterns (Figure S25). TGA was carried out under N_2 atmosphere and revealed that the framework of compound **5** is stable up to 200 °C (Figure S25).

Cu-shp-MOF-1 Platform. Encouraged by the ability to transplant the **alb** net into a chemically different MOF based on the use of the dodecacarboxylate ligand as the requisite hexagonal-prism building unit, we extended this approach to the **shp**-MOF platform. Understandably, the ability of the newly synthesized dodecacarboxylate ligand to mimic the d6R, by peripherally exposing the 12 carboxylates to resemble the requisite hexagonal-prism building unit, inspired us to transplant the **shp** topology into a copper-based MOF by employing the copper paddlewheel $[Cu_2(O_2C-)_4]$ cluster as the complementary square building unit, thus offering the potential to construct the first Cu-**shp**-MOF.

Indeed, reactions between $Cu(NO_3)_2{\cdot}2.5H_2O$ and H_{12}-HBCPB in DMF/pyridine solution yielded green hexagonal block-shaped crystals, formulated by SCXRD as $[Cu_6(C_{132}O_{30}H_{78})(H_2O)_6]{\cdot}(solv)_x$ (Cu-**shp**-MOF-1) (**6**) (Table S8). The SCXRD study revealed that compound **6** crystallizes in the hexagonal space group *P*6/*mcc*. Analysis of the resultant crystal structure of **6** revealed the *in situ* formation of the anticipated 4-c copper paddlewheel $[Cu_2(O_2C-)_4]$ building block and its subsequent assemblage by four separate fully deprotonated dodecacarboxylate ligands (HBCPB) to yield a new 3-periodic highly connected copper-based MOF (Cu-**shp**-MOF-1).

Topological analysis of the resulting crystal structure revealed that the deliberate combination of the aforementioned 4-c MBB, $[Cu_2(O_2C-)_4]$, and 12-c organic MBB, HBCPB ligand, resulted as envisioned in the formation of a highly connected MOF, the Cu-**shp**-MOF-1 structure based on the reticulation of the (4,12)-c net with **shp** underlying topology (Figure 1).

The conformation of the ligand in the Cu-**shp**-MOF-1 is similar to the linker conformation observed in the In-**alb**-MOF-1,

DOI: 10.1021/jacs.7b00219
J. Am. Chem. Soc. 2017, 139, 3265−3274

ultimately resulting in points of extension of the 12-c MBB to coincide with the vertices of the hexagonal-prism, the 12-c vertex figure of the **shp** net. From a purely topological point of view, this structure could alternatively be termed as the newly discovered **cez** topology: (3,4,6)-c trinodal net with minimal transitivity [32] (Figure 2), where the ligand can be deconstructed into one 3-c node and one 6-c node. This novel **cez** topology represents a new type of **shp**-derived nets.

Gas Sorption Studies of alb-MOF-1. The flexibility of crystalline porous MOFs is proven to be vital in various key applications such as methane storage, where the reversible transition/deformation is controlled via external stimuli, such as adsorption/desorption of guest molecules.[19] The flexible features of the Y-**alb**-MOF-1 (**3**) prompted us to investigate its gas adsorption properties and structural flexibility in the presence of different adsorbate probe molecules. Before the measurement, a freshly DMF-washed sample of **3** was exchanged with acetone over 3 days, and then the sample was activated under dynamic vacuum for 12 h. As illustrated in Figure 5, various gas molecules, such as N_2, Ar, CH_4, and CO_2, were employed as adsorbates, at their boiling point temperature, to evaluate the adsorption properties of the degassed Y-**alb**-MOF-1 and probe any plausible associated framework flexibility. The N_2, Ar, CH_4, and CO_2 gas sorption isotherms of compound **3** displayed a two-step adsorption behavior and a significant hysteresis, characteristic of a flexible framework (Figure 5). The amount of argon adsorbed up to the first plateau was estimated to be ca. 9.4 mmol·g^{-1} ($P/P_0 \approx 0.05$), and the total amount of argon adsorbed in the framework was estimated to be ca. 16.1 mmol·g^{-1} ($P/P_0 \approx 0.95$), equivalent to an uptake increase of nearly ca. 6.7 mmol·g^{-1} between the two adsorption plateaus. Accordingly, the apparent Langmuir surface area of Y-**alb**-MOF-1, determined using the Ar adsorption isotherm in 87 K and calculated using the Quantachrome software, assuming a value of 14.2 Å^2 for the molecular cross-sectional area of Ar, was estimated to be ca. 1550 m^2·g^{-1}. It should be noted that the apparent BET surface area cannot be precisely determined for the present framework due to the evident steps in the low-pressure region of the adsorption isotherms. The associated pore volumes of **3** derived from the Ar isotherm at the first and second plateaus were estimated to be ca. 0.27 cm^3·g^{-1} ($P/P_0 \approx 0.05$) and ca. 0.52 cm^3·g^{-1} ($P/P_0 \approx 0.95$), respectively. The estimated total pore volume from the second plateau correlates relatively with the calculated total pore volume from the single-crystal structure (0.63 cm^3·g^{-1}). The estimated total pore volumes accessible for **3** derived from the N_2, CH_4, and CO_2 adsorption isotherms at the first and second plateaus were found to be respectively ca. 0.29 cm^3·g^{-1} ($P/P_0 \approx 0.03$) and 0.56 cm^3·g^{-1} ($P/P_0 \approx 0.95$) for N_2, ca. 0.28 cm^3·g^{-1} ($P/P_0 \approx 0.03$) and 0.56 cm^3·g^{-1} ($P/P_0 \approx 0.95$) for CH_4, and ca. 0.37 cm^3·g^{-1} ($P/P_0 \approx 0.32$) and 0.66 cm^3·g^{-1} ($P/P_0 \approx 0.95$)) for CO_2.

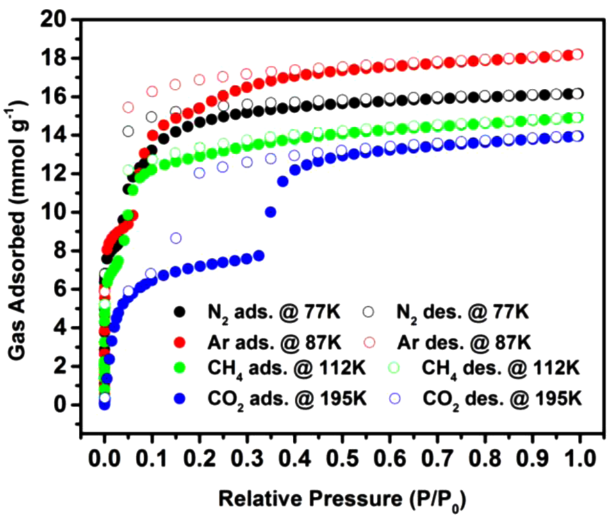

Figure 5. N_2, Ar, CH_4, and CO_2 sorption isotherms of the degassed Y-**alb**-MOF-1 (**3**) at their boiling point temperature. Color codes: N_2 sorption isotherm at 77 K (black); Ar sorption isotherm at 87 K (red); CH_4 sorption isotherm at 112 K (green); CO_2 sorption isotherm at 195 K (blue). Filled circles represent the adsorption, and open circles represent the desorption.

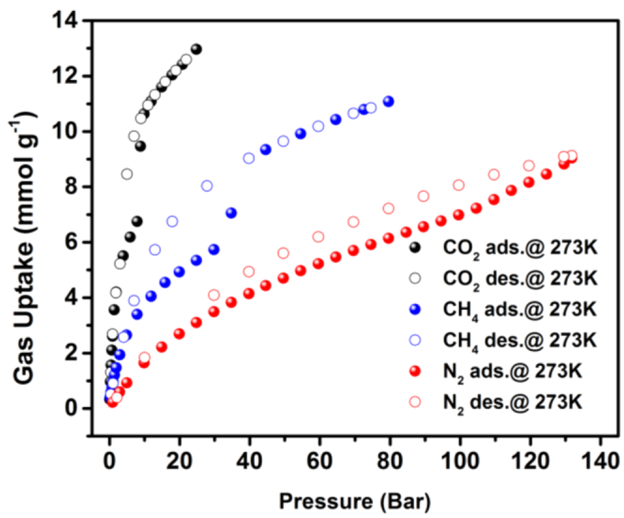

Figure 6. High-pressure CO_2 (black), CH_4 (blue), and N_2 (red) sorption isotherms for the degassed Y-**alb**-MOF-1 (**3**) at 273 K. Filled circles represent the adsorption, and open circles represent the desorption.

To gain a better understanding on the flexible nature of the Y-**alb**-MOF-1 (**3**), high-pressure gas adsorption studies were conducted in order to investigate/elucidate the transformation/relation between the closed (narrow-pore phase) and open states (large-pore phase). High-pressure CO_2, CH_4 and N_2 adsorption experiments were conducted at 273 K (Figure 6) and 298 K (Figure S52) up to 25, 80, and 130 bar, respectively. Since the sample has been activated and evacuated prior the gas sorption measurements, the framework should be in its contracted state. Accordingly, pressure and specifically adsorbed guest molecules can induce the framework to undergo a structural transition from a "closed" (narrow-pore) state to a relatively "open" (large-pore) state, leading to the observation/occurrence of breathing adsorption effect in the sorption process. In the CO_2 adsorption study, the original narrow-pore phase was altered/morphed to a relatively large-pore phase upon a plausible gate opening around 8 bar at 273 K, associated with CO_2 uptake of nearly 6.7 mmol·g^{-1}. In contrast, the apparent gate opening in the case of CH_4 as an adsorbate occurred around 30 bar at 273 K, with an associated CH_4 uptake around 5.8 mmol·g^{-1}. In the case of the N_2 adsorption study, the hysteresis is apparent, but the step is not well defined. Similar behaviors were observed for CO_2, CH_4, and N_2 at 298 K in high-pressure regions (Figure S52). These results clearly demonstrate and corroborate that the transformation between the "closed" (narrow-pore phase) and "open" (large-

DOI: 10.1021/jacs.7b00219
J. Am. Chem. Soc. 2017, 139, 3265−3274

pore phase) states is triggered by the adsorbed gas probe molecules and their density in the pores.

■ CONCLUSIONS

We reported the design and synthesis of two chemically distinct but topologically related highly connected MOFs based on the successful reticulation of binodal edge-transitive **shp** and **alb** nets.

We described the design and construction of a series of highly stable RE porphyrinic **shp**-MOFs based on the assembly of 12-connected nonanuclear carboxylate-based MBBs, displaying rare d6R building units, and 4-connected tetratopic ligands. Especially, we reported the rational design and deliberate assembly of the long-awaited (6,12)-c **alb**-MOFs, i.e., RE-**alb**-MOF-1 and In-**alb**-MOF-1. The In-**alb**-MOF-1 represents the first example of **alb**-MOFs based on the assembly of a metal trinuclear cluster and a purposely made 12-c dodecacarboxylate ligand. The successful construction of the first In-**alb**-MOF was the immediate result of the rational practice of reticular chemistry in combination with the understanding and deployment of net-coded building units (**net**-cBUs). The two **alb**-MOFs, related to the same parent **alb** topology, based on the combination of trigonal-prism and hexagonal-prism **net**-cBUs, were constructed by carrying out a topological transplantation, where building blocks in one **alb**-MOF (RE-**alb**-MOF-1, the 6-connected hexacarboxylate organic ligands and 12-connected inorganic RE polynuclear clusters) are replaced by chemically different but topologically related building blocks to construct a second **alb**-MOF (In-**alb**-MOF-1, the 6-connected inorganic indium trinuclear clusters and 12-connected dodecacarboxylate organic ligands).

Practically, the same approach was employed successfully to transplant the **shp** topology into a copper-based MOF by employing the copper paddlewheel $[Cu_2(O_2C-)_4]$ cluster as the complementary square building unit, thus allowing the construction of the first Cu-**shp**-MOF.

The four presented structures illustrate the importance of edge-transitive nets as appropriate blueprints, given the reaction conditions to generate the highly connected inorganic MBB *in situ* are isolated and/or the polytopic organic ligand encompasses the right connectivity that affords the positioning of coordinating moieties in the intricate and desired highly connected geometry for the design and directed assembly of MOFs. Most importantly, we revealed that the highly connected edge-transitive nets such **shp** and **alb** are ideal for the topological transplantation and the deliberate construction of related MOFs based on minimal edge-transitive nets.

The present study establishes an unprecedented control in the design and deliberate assembly of new MOF platforms, resulting from the conceptualization/employment of net-coded building units (**net**-cBUs), where precise embedded geometrical information codes uniquely and matchlessly a selected net, as a commanding route for the rational design of MOFs. Considerably superior control in the MOF design offers great potential for the development of made-to-order MOFs with on-demand/programmed properties to address the needs in various applications such as gas storage, gas/vapor separations, and chemical sensing.

■ EXPERIMENTAL SECTION

Synthesis of Y-shp-MOF-1 (1). A solution of $Y(NO_3)_3 \cdot 6H_2O$ (21.9 mg, 0.06 mmol) and H_4TCPP (7.9 mg, 0.01 mmol) in 1.5 mL of DMF and 0.5 mL of H_2O was placed in a 20 mL scintillation vial. Next, 2 mL of 4 M 2-FBA in DMF was added to the mixture, which was then sonicated for 30 min. The resultant mixture was sealed in the vial and heated to 115 °C for 24 h. The dark red crystals obtained were filtered and washed with DMF. The as-synthesized material was found to be insoluble in H_2O and common organic solvents. Crystals were harvested, soaked in DMF overnight, and then exchanged in MeOH for 3 days. Note that the MeOH solution was refreshed at least every 12 h. (Yield: 7.8 mg, 76% based on ligand.)

Synthesis of Y-shp-MOF-1 (Zn) (1-Zn). A solution of $Y(NO_3)_3 \cdot 6H_2O$ (21.9 mg, 0.06 mmol) and H_4TCPP (7.9 mg, 0.01 mmol) in 1.5 mL of DMF and 0.5 mL of H_2O was placed in a 20 mL scintillation vial. Next, 2 mL of 4 M FBA in DMF and 0.3 mL of 0.04 M $ZnCl_2$ in DMF were added to the mixture, which was then sonicated for 30 min. The resultant mixture was sealed in the vial and heated to 115 °C for 24 h. The dark red crystals were filtered and washed with DMF. The as-synthesized material was found to be insoluble in H_2O and common organic solvents. Crystals were harvested, soaked in DMF overnight, and then exchanged in MeOH for 3 days. Note that the MeOH solution was refreshed at least every 12 h. (Yield: 8.8 mg, 66% based on ligand.)

Synthesis of Y-shp-MOF-1 (Fe) (1-Fe). A solution of $Y(NO_3)_3 \cdot 6H_2O$ (18.3 mg, 0.05 mmol) and FeTCPPCl (8.8 mg, 0.01 mmol) in 1.5 mL of DMF and 0.5 mL of H_2O was placed in a 20 mL scintillation vial. Next, 150 μL of concentrated acetic acid (AcOH) and 2 mL of 4 M FBA in DMF were added to the mixture, which was then sonicated for 30 min. The resultant mixture was sealed in the vial and heated to 115 °C for 24 h. The obtained dark brown crystals were filtered and washed with DMF. The as-synthesized material was found to be insoluble in H_2O and common organic solvents. Crystals were harvested, soaked in DMF overnight, and then exchanged in MeOH for 3 days. Note that the MeOH solution was refreshed at least every 12 h. (Yield: 8.9 mg, 66% based on ligand.)

Synthesis of Tb-shp-MOF-1 (2). A solution of $Tb(NO_3)_3 \cdot 5H_2O$ (26.1 mg, 0.06 mmol) and H_4TCPP (7.9 mg, 0.01 mmol) in 1.5 mL of DMF and 0.5 mL of H_2O was placed in a 20 mL scintillation vial. Next, 2 mL of 4 M FBA in DMF was added to the mixture, which was then sonicated for 30 min. The resultant mixture was sealed in the vial and heated to 115 °C for 24 h. The obtained dark red crystals were filtered and washed with DMF. The as-synthesized material was found to be insoluble in H_2O and common organic solvents. Crystals were harvested, soaked in DMF overnight, and then exchanged in MeOH for 3 days. Note that the MeOH solution was refreshed at least every 12 h. (Yield: 7.8 mg, 76% based on ligand.)

Synthesis of Y-alb-MOF-1 (3). A solution of $Y(NO_3)_3 \cdot 6H_2O$ (29.2 mg, 0.08 mmol) and H_6Me-TDCPB (10.7 mg, 0.01 mmol) in 2 mL of DMF, 0.5 mL of chlorobenzene, and 1 mL of H_2O was placed in a 20 mL scintillation vial. Next, 1 mL of 4 M FBA in DMF was added to the mixture, which was then sonicated for 30 min. The resultant mixture was sealed in the vial and heated to 105 °C for 72 h. The obtained pure colorless block crystals were filtered and washed with DMF three times. The as-synthesized material was found to be insoluble in H_2O and common organic solvents. Crystals were harvested, soaked in DMF overnight, and then exchanged in acetone for 3 days. Note that the acetone solution was refreshed at least every 12 h. (Yield: 13.1 mg, 80% based on ligand.)

Synthesis of Tb-alb-MOF-1 (4). A solution of $Tb(NO_3)_3 \cdot 5H_2O$ (34.8 mg, 0.08 mmol) and H_6Me-TDCPB (10.7 mg, 0.01 mmol) in 2 mL of DMF, 0.5 mL of chlorobenzene, and 1 mL of H_2O was placed in a 20 mL scintillation vial. Next, 1 mL of 4 M FBA in DMF was added to the mixture, which was then sonicated for 30 min. The mixture was sealed in the vial and heated to 105 °C for 72 h. The obtained pure colorless block crystals were filtered and washed with DMF three times. The as-synthesized material was found to be insoluble in H_2O and common organic solvents. Crystals were harvested, soaked in DMF overnight, and then exchanged in acetone for 3 days. Note that the acetone solution was refreshed at least every 12 h. (Yield: 14.3 mg, 77% based on ligand.)

Synthesis of In-alb-MOF-1 (5). A solution of $In(NO_3)_3 \cdot 2H_2O$ (13.5 mg, 0.04 mmol) and H_{12}HBCPB (5.4 mg, 0.0025 mmol) in 1.5 mL of DMF and 1 mL of acetonitrile was placed in a 20 mL scintillation vial. Next, 2 mL of 3.5 M HNO_3 in DMF was added to the mixture,

DOI: 10.1021/jacs.7b00219
J. Am. Chem. Soc. 2017, 139, 3265−3274

which was then sonicated for 30 min. The resultant mixture was sealed in the vial and heated to 105 °C for 48 h. The obtained pure colorless block crystals were filtered and washed with DMF three times. The as-synthesized material was found to be insoluble in H_2O and common organic solvents. Crystals were harvested, soaked in DMF overnight, and then exchanged in acetone for 3 days. Note that the acetone solution was refreshed at least every 12 h. (Yield: 8.3 mg, 60% based on ligand.)

Synthesis of Cu-shp-MOF-1 (6). A solution of $Cu(NO_3)_2{\cdot}2.5H_2O$ (14.0 mg, 0.06 mmol) and H_{12}HBCPB (10.8 mg, 0.005 mmol) in 2.5 mL of DMF was prepared in a 20 mL scintillation vial. Next, 0.5 mL of 3.5 M HNO_3 in DMF and 0.5 mL of pyridine were added to the mixture, which was then sonicated for 20 min. The resultant mixture was sealed in the vial and heated to 115 °C for 72 h. The obtained green hexagonal block crystals were filtered and washed with DMF. The as-synthesized material was determined to be insoluble in H_2O and common organic solvents. (Yield: 8.5 mg, 64% based on ligand.)

■ ASSOCIATED CONTENT

Supporting Information

The Supporting Information is available free of charge on the ACS Publications website at DOI: 10.1021/jacs.7b00219.

Detailed procedures for the synthesis of the organic ligands, PXRD, TGA, additional structural figures, and adsorption isotherms, including Figures S1−S54 and Tables S1−S13 (PDF)

Single-crystal X-ray diffraction data for 1, 1-Fe, 1-Zn, 2, 3, 4, 5, and 6 (CIF)

■ AUTHOR INFORMATION

Corresponding Author

*mohamed.eddaoudi@kaust.edu.sa

ORCID

Łukasz J. Weseliński: 0000-0003-4516-2727

Dong-Xu Xue: 0000-0003-1938-9055

Mohamed Eddaoudi: 0000-0003-1916-9837

Notes

The authors declare no competing financial interest.

■ ACKNOWLEDGMENTS

Research reported in this publication was supported by King Abdullah University of Science and Technology (KAUST).

■ REFERENCES

(1) (a) Furukawa, H.; Cordova, K. E.; O'Keeffe, M.; Yaghi, O. M. *Science* **2013**, *341*, 1230444. (b) Kitagawa, S.; Kitaura, R.; Noro, S.-i. *Angew. Chem., Int. Ed.* **2004**, *43*, 2334−2375. (c) Ferey, G. *Chem. Soc. Rev.* **2008**, *37*, 191−214.

(2) (a) Mason, J. A.; Oktawiec, J.; Taylor, M. K.; Hudson, M. R.; Rodriguez, J.; Bachman, J. E.; Gonzalez, M. I.; Cervellino, A.; Guagliardi, A.; Brown, C. M.; Llewellyn, P. L.; Masciocchi, N.; Long, J. R. *Nature* **2015**, *527*, 357−361. (b) Nugent, P.; Belmabkhout, Y.; Burd, S. D.; Cairns, A. J.; Luebke, R.; Forrest, K.; Pham, T.; Ma, S.; Space, B.; Wojtas, L.; Eddaoudi, M.; Zaworotko, M. J. *Nature* **2013**, *495*, 80−84.

(3) (a) Liu, J.; Chen, L.; Cui, H.; Zhang, J.; Zhang, L.; Su, C.-Y. *Chem. Soc. Rev.* **2014**, *43*, 6011−6061. (b) Kornienko, N.; Zhao, Y.; Kley, C. S.; Zhu, C.; Kim, D.; Lin, S.; Chang, C. J.; Yaghi, O. M.; Yang, P. *J. Am. Chem. Soc.* **2015**, *137*, 14129−14135. (c) Mondloch, J. E.; Katz, M. J.; Isley, W. C.; Ghosh, P.; Liao, P.; Bury, W.; Wagner, G. W.; Hall, M. G.; DeCoste, J. B.; Peterson, G. W.; Snurr, R. Q.; Cramer, C. J.; Hupp, J. T.; Farha, O. K. *Nat. Mater.* **2015**, *14*, 512−516.

(4) Huxford, R. C.; Della Rocca, J.; Lin, W. *Curr. Opin. Chem. Biol.* **2010**, *14*, 262−268.

(5) (a) Cui, Y.; Yue, Y.; Qian, G.; Chen, B. *Chem. Rev.* **2012**, *112*, 1126−1162. (b) Hu, Z.; Deibert, B. J.; Li, J. *Chem. Soc. Rev.* **2014**, *43*, 5815−5840. (c) Kreno, L. E.; Leong, K.; Farha, O. K.; Allendorf, M.; Van Duyne, R. P.; Hupp, J. T. *Chem. Rev.* **2012**, *112*, 1105−1125.

(6) (a) Eddaoudi, M.; Moler, D. B.; Li, H.; Chen, B.; Reineke, T. M.; O'Keeffe, M.; Yaghi, O. M. *Acc. Chem. Res.* **2001**, *34*, 319−330. (b) Alezi, D.; Belmabkhout, Y.; Suyetin, M.; Bhatt, P. M.; Weseliński, Ł. J.; Solovyeva, V.; Adil, K.; Spanopoulos, I.; Trikalitis, P. N.; Emwas, A.-H.; Eddaoudi, M. *J. Am. Chem. Soc.* **2015**, *137*, 13308−13318. (c) Xue, D.-X.; Cairns, A. J.; Belmabkhout, Y.; Wojtas, Ł.; Liu, Y.; Alkordi, M. H.; Eddaoudi, M. *J. Am. Chem. Soc.* **2013**, *135*, 7660−7667. (d) Guillerm, V.; Kim, D.; Eubank, J. F.; Luebke, R.; Liu, X.; Adil, K.; Lah, M. S.; Eddaoudi, M. *Chem. Soc. Rev.* **2014**, *43*, 6141−6172. (e) Eddaoudi, M.; Sava, D. F.; Eubank, J. F.; Adil, K.; Guillerm, V. *Chem. Soc. Rev.* **2015**, *44*, 228−249.

(7) Li, M.; Li, D.; O'Keeffe, M.; Yaghi, O. M. *Chem. Rev.* **2014**, *114*, 1343−1370.

(8) (a) Guillerm, V.; Weseliński, Ł. J.; Belmabkhout, Y.; Cairns, A. J.; D'Elia, V.; Wojtas, Ł.; Adil, K.; Eddaoudi, M. *Nat. Chem.* **2014**, *6*, 673−680. (b) Liu, T. F.; Feng, D.; Chen, Y. P.; Zou, L.; Bosch, M.; Yuan, S.; Wei, Z.; Fordham, S.; Wang, K.; Zhou, H. C. *J. Am. Chem. Soc.* **2015**, *137*, 413−9. (c) Feng, D.; Gu, Z.-Y.; Chen, Y.-P.; Park, J.; Wei, Z.; Sun, Y.; Bosch, M.; Yuan, S.; Zhou, H.-C. *J. Am. Chem. Soc.* **2014**, *136*, 17714−17717.

(9) (a) Luebke, R.; Belmabkhout, Y.; Weseliński, Ł. J.; Cairns, A. J.; Alkordi, M.; Norton, G.; Wojtas, L.; Adil, K.; Eddaoudi, M. *Chem. Sci.* **2015**, *6*, 4095−4102. (b) Alezi, D.; Peedikakkal, A. M. P.; Weseliński, Ł. J.; Guillerm, V.; Belmabkhout, Y.; Cairns, A. J.; Chen, Z.; Wojtas, Ł.; Eddaoudi, M. *J. Am. Chem. Soc.* **2015**, *137*, 5421−5430.

(10) (a) O'Keeffe, M.; Peskov, M. A.; Ramsden, S. J.; Yaghi, O. M. *Acc. Chem. Res.* **2008**, *41*, 1782−1789. (b) Delgado-Friedrichs, O.; O'Keeffe, M.; Yaghi, O. M. *Acta Crystallogr., Sect. A: Found. Crystallogr.* **2006**, *62*, 350−355.

(11) Humphrey, S. M.; Mole, R. A.; McPartlin, M.; McInnes, E. J. L.; Wood, P. T. *Inorg. Chem.* **2005**, *44*, 5981−5983.

(12) (a) Férey, G.; Mellot-Draznieks, C.; Serre, C.; Millange, F.; Dutour, J.; Surblé, S.; Margiolaki, I. *Science* **2005**, *309*, 2040−2042. (b) Liu, Y.; Eubank, J. F.; Cairns, A. J.; Eckert, J.; Kravtsov, V. C.; Luebke, R.; Eddaoudi, M. *Angew. Chem., Int. Ed.* **2007**, *46*, 3278−3283.

(13) (a) Chae, H. K.; Eddaoudi, M.; Kim, J.; Hauck, S. I.; Hartwig, J. F.; O'Keeffe, M.; Yaghi, O. M. *J. Am. Chem. Soc.* **2001**, *123*, 11482−11483. (b) Jia, J.; Sun, F.; Ma, H.; Wang, L.; Cai, K.; Bian, Z.; Gao, L.; Zhu, G. *J. Mater. Chem. A* **2013**, *1*, 10112−10115.

(14) Spek, A. *Acta Crystallogr., Sect. D: Biol. Crystallogr.* **2009**, *65*, 148−155.

(15) Gándara, F.; Furukawa, H.; Lee, S.; Yaghi, O. M. *J. Am. Chem. Soc.* **2014**, *136*, 5271−5274.

(16) Li, B.; Wen, H.-M.; Wang, H.; Wu, H.; Tyagi, M.; Yildirim, T.; Zhou, W.; Chen, B. *J. Am. Chem. Soc.* **2014**, *136*, 6207−6210.

(17) Peng, Y.; Krungleviciute, V.; Eryazici, I.; Hupp, J. T.; Farha, O. K.; Yildirim, T. *J. Am. Chem. Soc.* **2013**, *135*, 11887−11894.

(18) Mason, J. A.; Veenstra, M.; Long, J. R. *Chem. Sci.* **2014**, *5*, 32−51.

(19) (a) Horike, S.; Shimomura, S.; Kitagawa, S. *Nat. Chem.* **2009**, *1*, 695−704. (b) Lin, Z.-J.; Lu, J.; Hong, M.; Cao, R. *Chem. Soc. Rev.* **2014**, *43*, 5867−5895. (c) Schneemann, A.; Bon, V.; Schwedler, I.; Senkovska, I.; Kaskel, S.; Fischer, R. A. *Chem. Soc. Rev.* **2014**, *43*, 6062−6096.

DOI: 10.1021/jacs.7b00219
J. Am. Chem. Soc. 2017, 139, 3265−3274